# Lithium-assisted Exfoliation and Photoelectrocatalytic Water Splitting of 2D Palladium Thiophosphate

Wu, B.; Kempt, R.; Kovalska, E.; Luxa, J.; Kuc, A. B.; Heine, T.; Sofer, Z.;

Originally published:

January 2021

**ACS Applied Nano Materials 4(2021), 441-448**

DOI: https://doi.org/10.1021/acsanm.0c02775

# Lithium-assisted Exfoliation and Photoelectrocatalytic Water Splitting of 2D Palladium Thiophosphate

| | |
|---|---|
| Journal: | *ACS Applied Nano Materials* |
| Manuscript ID | an-2020-027753 |
| Manuscript Type: | Article |
| Date Submitted by the Author: | 16-Oct-2020 |
| Complete List of Authors: | Wu, Bing; Vysoka skola chemicko-technologicka v Praze, Inorganic Chemistry<br>Kempt, Roman; TU Dresden<br>Kovalska, Evgeniya; Vysoka skola chemicko-technologicka v Praze, Inorganic Chemistry<br>Luxa, Jan; Vysoka skola chemicko-technologicka v Praze,<br>Kuc, Agnieszka; Helmholtz-Zentrum Dresden-Rossendorf,<br>Heine, Thomas; TU Dresden, School of Science<br>Sofer, Zdeněk; Vysoka skola chemicko-technologicka v Praze, Inorganic Chemistry |
| | |

# Lithium-assisted Exfoliation and Photoelectrocatalytic Water Splitting of 2D Palladium Thiophosphate

*Bing Wu[1], Roman Kempt[2], Evgeniya Kovalska[1], Jan Luxa[1], Agnieszka Kuc[3], Thomas Heine[2], Zdenek Sofer[1]**

[1] Department of Inorganic Chemistry, University of Chemistry and Technology, Prague, Technická 5, 166 28 Prague 6, Czech Republic

[2] Technische Universität Dresden, Chair of Theoretical Chemistry, Bergtrasse 66c, 01062, Dresden, Germany

[3] Helmholtz-Zentrum Dresden-Rossendorf, Institute of Resource Ecology, Permoserstr. 15, 04318, Leipzig, Germany

**Abstract**

Efficient photoelectrocatalytic (PEC) water splitting could be the solution for environmental and energy problems on planet Earth. Here, we explore 2D palladium thiophosphate $Pd_3(PS_4)_2$, which is a promising photocatalyst absorbing light in the visible range. We obtain a few-layer $Pd_3(PS_4)_2$ through lithium-assisted exfoliation from the bulk phase and characterize it employing Raman spectroscopy, XPS, AFM, and STM combined with DFT calculations. The measured band gap for as-obtained few-layer $Pd_3(PS_4)_2$ is 2.57 eV (indirect) and its band edges span the electrochemical potentials of the hydrogen and oxygen evolution reactions. The performance in the water-splitting reaction is studied under acidic, neutral, and alkaline conditions under

violet irradiation at 420 nm. 2D palladium phosphochalcogenides semiconductor with bifunctional electrocatalytic and photoelectrocatalytic properties. Our results show competitive performance compared with industrial Pt/C catalysts for solar-driven water splitting under acidic and alkaline conditions.

**Introduction**

Two-dimensional (2D) semiconductor photocatalysts are promising materials for the water-splitting reaction to generate hydrogen and oxygen – a sustainable supply of clean and renewable energy.[1-4] Compared with their three-dimensional (3D) bulk counterparts, the corresponding 2D nanosheets provide a high specific surface area and a low diffusion distance between the surface and the photogenerated electrons and holes, making them promising for the next generation of photocatalysts.[5-6] A material for photoelectrocatalytic (PEC) water splitting should satisfy the following requirements: (i) The band gap should be larger than the potential difference of 1.23 eV to split water, but smaller than 3.00 eV to harvest visible light properly; (ii) the conductive and valence bands must span the redox potential of water; (iii) the potential difference between the conduction band maximum (valence band minimum) and reduction (oxidation) potential ensures substantial reducing (oxidizing) power, but low overpotentials.[7-10] Several 2D semiconductor materials show excellent performance for PEC, which can further be boosted by chemical modifications. These include transition-metal chalcogenides, graphene-based materials, platinum-group layered materials etc. [11-19]

The compound $Pd_3(PS_4)_2$, a palladium thiophosphate with a layered, interdigitated structure, was first fabricated by chemical vapor transport (CVT) method in 1971.[20]

This study noted unsuitable photocatalytic properties of bulk $Pd_3(PS_4)_2$. On the other hand, first-principle calculations suggested that mono- and bilayer $Pd_3(PS_4)_2$ are promising photocatalysts.[21] In 2018, Zhang et al. reported an amorphous ultrasmall lithium-incorporated $Pd_3(PS_4)_2$.[22] Such an amorphous ultrasmall structure could enhance the electrocatalytic activity towards the hydrogen evolution reaction (HER). First-principles calculations predicted the stability of mono-, bi-, and trilayer $Pd_3(PS_4)_2$, with a layer-number dependent band gap between 2.5 - 3.0 eV and the band edges spanning the redox potential of water, which makes it a promising photocatalyst for the water splitting reaction.[21, 23-24] To date, the successful exfoliation of few-layer $Pd_3(PS_4)_2$ has not been reported.

Here, we report the exfoliation of few-layer palladium thiophosphate $Pd_3(PS_4)_2$ in solution from its bulk crystal via lithium intercalation and mild ultrasonication as shown in Scheme 1.[25] Firstly, the Li-ions were intercalated into the layers of bulk crystal in nonpolar hexane by continuous sonication, followed by solvation in highly polar DMSO to form a big solvated Li@DMSO group, which could effectively weaken the van der Waals forces between the 2D $Pd_3(PS_4)_2$ layers. Thus, exfoliated few-layer palladium thiophosphate sample could be achieved under further mild sonication. The red-purple bulk crystals (**Fig. S1**a) were grown by CVT.[20] We measured the valence band position and an indirect band gap of 2.57 eV, indicating the suitability of the material for photoelectrocatalytic water splitting, which is confirmed by DFT calculations. We further studied the electrochemical performance of HER and OER (oxygen evolution reaction) at pH=0, pH=7 and pH=14 under violet irradiation at 420

nm.

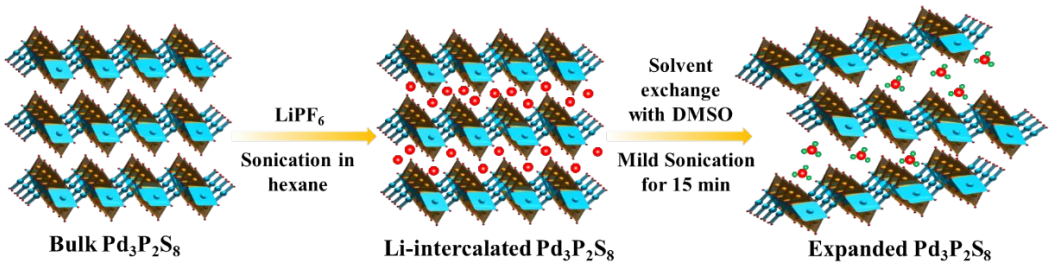


**Scheme 1.** Reaction scheme for the fabrication of exfoliated few-layer $Pd_3(PS_4)_2$.

## Experimental Section

### Chemicals

Palladium powder (99.99%) and red phosphorus (99.999%) were obtained from Mateck. Sulfur (99.999%) was obtained from Strem, Germany. $LiPF_6$ (99.9%) was obtained from Sigma-Aldrich, Czech Republic. Hexane, dimethylsulfoxide, sulfuric acid (96%), potassium hydroxide (KOH), sodium sulfate ($Na_2SO_4$), ammonium hydrogen phosphate ($(NH_4)_2HPO_4$) and ammonium dihydrogen phosphate ($NH_4H_2PO_4$) were obtained from Penta (Czech Republic) as analytical grade reagents. Phosphate buffer solution (PBS) was made by $(NH_4)_2HPO_4$ and $NH_4H_2PO_4$.

### Synthesis of $Pd_3(PS_4)_2$ crystals

Palladium, phosphorus and sulfur corresponding to 5g of the stoichiometric mixture were placed in quartz glass ampoule (20x100mm) and sealed under high vacuum ($1x10^{-5}$ mbar) by oxygen-hydrogen torch. The ampoule was heated in muffle furnace on 750 °C for 14 days. Formed dark red crystals were mechanically separated from ampoule in glovebox.

### Exfoliation of $Pd_3(PS_4)_2$ crystals

Firstly, 30 mg of $Pd_3(PS_4)_2$ bulk powder was dispersed in hexane solution (20 mL)

containing an anhydrous $LiPF_6$ at 1:1.2 molar ratio. The mixture was sonicated using an ultrasonic bath with a duration of 2 h to get Li-intercalated materials. The resulting dispersion was centrifuged at 1000 rpm to remove hexane and unreacted $LiPF_6$. Wet precipitate was dispersed into polar solvent DMSO to have the lithium ion which was intercalated into the layer of material solvated, followed by centrifugation and repeatedly washing for three times using DMSO. Finally, the sediments were put into DMSO and followed by mild sonication for 15 min to get the exfoliated $Pd_3(PS_4)_2$. The claybank color dispersion of exfoliated $Pd_3(PS_4)_2$ (**Fig. S1**b) was centrifuged at 5000 rpm for 30 min, then collecting exfoliated sample in supernatant liquid for further characterization.

**Characterization of materials**

The crystal pattern and structure were characterized using X-ray diffractometer (XRD, Bruker D8 with Cu Kα radiation, Germany) and transmission electron microscopy (TEM, EFTEM Jeol 2200 FS microscope, Japan). The XRD curve was fitted using Rietveld method by GSAS software.[26-27] Scanning electron microscopy (SEM, Tescan MAIA 3, Czech Republic), scanning transmission electron microscopy (STEM, Tescan MAIA 3, Czech Republic), and atomic force microscopy (AFM, Ntegra Spectra, NT-MDT, Russia) were conducted to characterize the morphology of the materials. The analysis of chemical composition and valence were done by energy dispersive spectroscopy (EDX, Oxford Instrument, England) and X-ray photoelectron spectrometer (XPS, SPECS, Germany). Raman spectra were measured using inVia Raman Microscope (Renishaw, England) in a backscattering geometry with a CCD

camera detector and DPSS laser (532 nm, 50 mW) with 5% laser power and 20× objectives. The particles size distribution was collected by Zetasizer ZSP (Malvern Panalytical, England). Visible light absorption spectra were recorded in solution by BLACK-Comet UV-Vis Spectrometer (StellarNet, United States).

**Electrochemical analysis**

The electrochemical measurements were conducted on Autolab PGSTAT204 (Eco Chemie, Utrecht, The Netherlands) controlled by NOVA 2.1 software (Eco Chemie) consisting of a three-electrode system. In Mott-Schottky (MS) experiments, 6 μL sample mixture (0.2 mg $mL^{-1}$) was drop-casted onto the surface (0.3 cm diameter) of precleaned glassy carbon (GC) electrode and was vacuum-dried as working electrode. A saturated Ag/AgCl electrode (SSCE) and a platinum plate respectively were used as reference and counter electrodes. The supporting electrolyte was 0.5 M $Na_2SO_4$ aqueous solution (pH 7.0). The MS plot was constructed at a fixed frequency of range from 100 to 200 Hz as a function of potential around open-circuit potential (OCP). The electrochemical impedance spectroscopy (EIS) measurements were implemented at the frequency range of 0.01 to 1000000 Hz with 0.1 V sinusoidal perturbations. A 4 series-connected 420 nm Ultraviolet LEDs with 2500 mW @ 500 mA was used for irradiation.

**Evaluation of pH-dependent photoelectrocatalytic water-splitting activity**

An 80 mL supporting electrolyte, at different pH values of 0.5 M $H_2SO_4$, 1 M PBS (pH 7.0, prepared by $(NH_4)_2HPO_4$ and $NH_4H_2PO_4$) and 1 M KOH aqueous solution, containing 1.2 μg of materials were placed to a 100 mL reactor with a temperature-controlled water bath at 25 °C. A 4 series-connected 420 nm violet LEDs with 2500

mW @ 500 mA were used for irradiation. The onset overpotential is defined at the current density of 10.0 mA $cm^{-2}$ for HER or OER. All applied potentials were converted to a reversible hydrogen electrode (RHE) by adding a value of (0.2224 + 0.059 × pH).

**Computational Methods**

Full structural optimization (relaxation of lattice vectors and atomic positions) were performed in FHI-AIMS[28] employing the PBE functional[29] on *light* tier 2 numeric atom-centered orbitals, including the many-body dispersion correction (MBD)[30] and scalar relativistic corrections (ZORA) on a 8x8(x6) Γ-centered *k*-grid. Band structures and densities of states were calculated including spin-orbit coupling (SOC) employing the HSE06 functional[31] on *tight* tier 1 numeric atom-centered orbitals with added auxiliary diffuse basis functions. Raman spectra were predicted employing a Coupled Perturbed Kohn-Sham approach[32] in Crystal17[33] including corrections for experimental conditions of 532 nm and 295 K.

**Results and discussion**

$Pd_3(PS_4)_2$ crystals of red-purple color[20] (**Fig. S1**a) were fabricated using CVT (see Methods). Powder XRD and Rietveld analysis confirmed the phase of tripalladium-di-tetrathiophosphate in space group $\mathbf{P\bar{3}}m1$ with the lattice parameters $a = b = 6.9079$ (10) Å and $c = 7.2885(3)$ Å, which is in good agreement with the literature and the predictions from theory (see **Fig. S**2a and Table 1).[20] The chemical composition was identified via EDS-mapping. The EDS spectrum (**Fig. S2**b-d) shows an elemental composition of 2.8:2:7.9, close to the theoretical stoichiometry of 3: 2: 8 of Pd: P: S. SEM images of the as-prepared material indicate a lamellar stacking of exfoliated

nanoflakes (**Fig. 1**a). The AFM images of the samples collected after the centrifugation at 5000 rpm for 30 min showed a thickness of 0.7 to 2 nm, (**Fig. 1**b-c). The exfoliated nanoflakes show a lateral size of about 100 nm based on AFM and STEM (**Fig. S3**c) analysis, which is close to the size (**Fig. S3**a) measured by dynamic light scattering method with an average distribution around 74.91 nm. The EDS spectrum of the exfoliated $Pd_3(PS_4)_2$ (**Fig. S3**d) indicates a stoichiometry of 3: 2: 8 of Pd: P: S, correspondingly.

The EDX-mapping (**Fig. S3e**) shows the presence and uniform distribution of Pd, P and S in the $Pd_3(PS_4)_2$ nanosheets selected from TEM image (**Fig. 1**d). The corresponding high-resolution TEM (HRTEM) image of a typical $Pd_3(PS_4)_2$ sheet reveals the well-crystalline structure without visible defects. The distances between the miller planes (100) and (200) were measured to be 0.591 and 0.303 nm, respectively, agreeing with the literature. **Fig. 1**e depicts the crystal plane structures of a single layer of $Pd_3(PS_4)_2$ with the (100) and (200) planes, where the distance between the (100) planes equals the sum of two (200) planes.

As shown in the XRD in **Fig. S3b**, the (001) peak of $Pd_3(PS_4)_2$ shifts from 12.53° for the bulk to 11.87° for the exfoliated material, meanwhile only the (001) peak exists with a weaker intensity and other peaks disappear in the exfoliated $Pd_3(PS_4)_2$. This phenomenon occurs typically in the 2D materials after being exfoliated into few layers.[34-35]

**Fig. 1**f shows the Raman spectra measured for the bulk and exfoliated material as well as the calculated spectra for different layer numbers. The $E_g^1/A_{1g}^1$ signals around

200 $cm^{-1}$ and the $E_g^3$ signal at 316 $cm^{-1}$ are characteristic for this material. They correspond to vibration modes of the tetrathiophosphate units (see **Fig. 1**g), and are in good agreement with the literature[36] and theory. The $A_{1g}^3$ mode corresponds to the P-S-bond stretching and is visible at 720 $cm^{-1}$ in the bulk sample, but disappears for fewer layers as predicted by the calculation. Furthermore, the $E_g^3$ mode shifts by 1.7 $cm^{-1}$ to lower wavenumbers in the exfoliated sample compared to the bulk sample, which agrees with the prediction from theory for fewer layers. The Raman spectra revealed that the structure of $Pd_3(PS_4)_2$ is maintained after exfoliation.

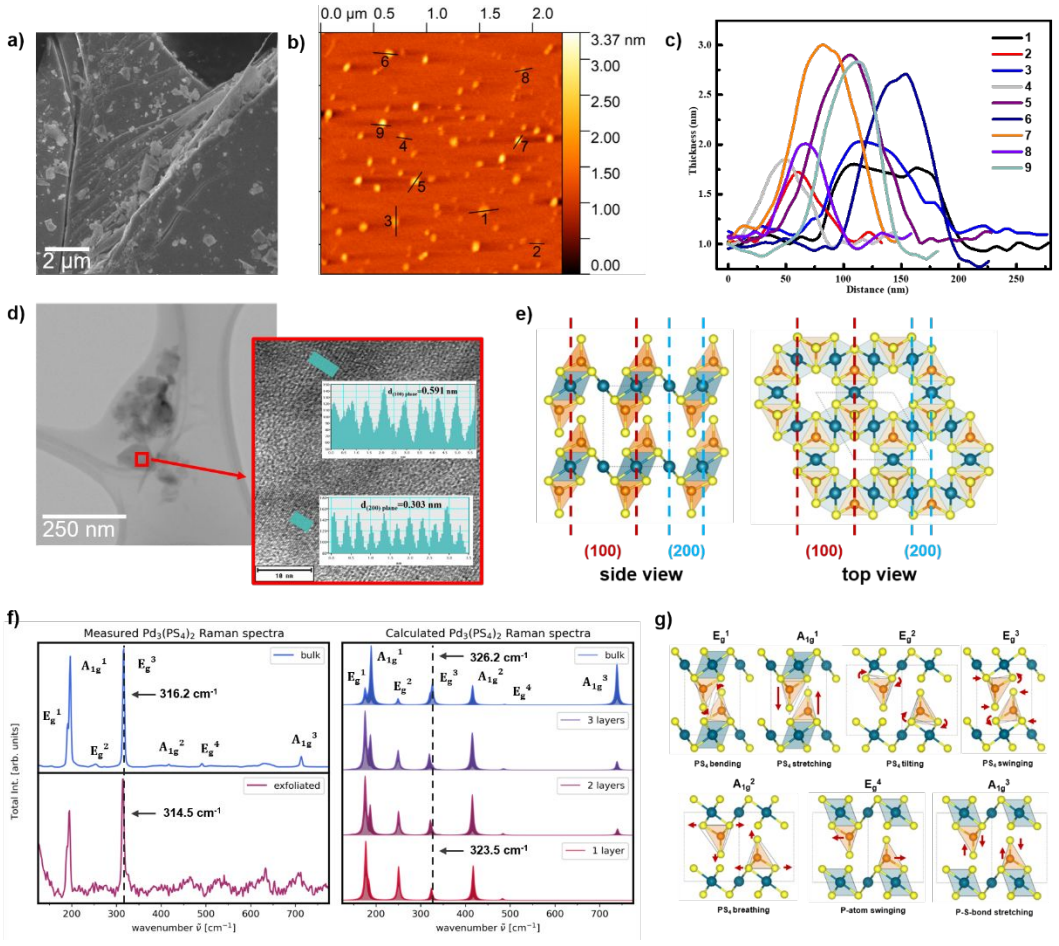


**Figure 1** Morphology and structure characterization of bulk and exfoliated $Pd_3(PS_4)_2$: (a) SEM image of bulk $Pd_3(PS_4)_2$; (b) AFM image of exfoliated $Pd_3(PS_4)_2$ and (c) corresponding thickness of selected nanosheets; (d) TEM image and (e) visualization of the structure with given lattice planes; (f) Measured and calculated Raman spectra; (g) Raman modes.

Additionally, we performed X-ray photoelectron spectroscopy (XPS) to investigate surface oxidation. **Fig. S**4 shows the XPS survey spectra of Pd, P, S O and C elements of both bulk and exfoliated $Pd_3(PS_4)_2$ samples.[22] For bulk material, the Pd 3d core-level XPS spectra (**Fig. S4**b) demonstrates doublet peaks at around 337.1 and 342.2 eV, corresponding to the Pd $3d_{5/2}$ and $3d_{3/2}$ levels, respectively, where the spin-orbit components separated by about 5.1 eV are in a good agreement with previous reports.[37] Note that the decomposition of the peak located at about 341.5 and 336.3 eV in the Pd 3d XPS core spectrum of the bulk sample could be ascribed to the existence of surface oxidation to $PdO_y$. The S 2p XPS core-level spectrum (**Fig. S4**c), spin-orbit doublet at 163.4 eV and 162.2 eV of S $2p_{1/2}$ and S $2p_{3/2}$ separated by 1.2 eV is in a good agreement with the value reported for the chalcogenides.[38] As for the P 2p core-level XPS spectrum (**Fig. S4**d), the peaks at about 132.2 eV and 131.1 eV correspond to the P $2p_{3/2}$ and P $2p_{1/2}$ spin-orbit. Moreover, the XPS spectrums for all elements of obtained $Pd_3(PS_4)_2$ nanosheets show no apparent shift compared to the bulk sample.

Strong visible light absorption is crucial for efficient photocatalysis. We performed UV-Vis measurements to obtain diffuse reflectance spectra to study the absorption properties of $Pd_3(PS_4)_2$. As seen in **Fig. 3**a, the exfoliated $Pd_3(PS_4)_2$ shows a significant light absorption under 482.5 nm. Furthermore, the band gap ($E_g$) of as-prepared $Pd_3(PS_4)_2$-based photocatalyst was calculated using the Eq. (1):

$$(ahv)^n = A(hv - Eg) \quad (1)$$

where $\alpha$, $h$, $v$, $A$, $Eg$ are the absorption coefficient, Planck's constant, light frequency, proportionality constant and optical band gap energy, respectively. The $n$ is a constant

determined by the type of optical transition. It is equal to 4 for an indirect transition and 1 for a direct transition.[39] As shown in **Fig. 3**a, the indirect band gap of exfoliated $Pd_3(PS_4)_2$ was measured to be 2.57 eV. Meanwhile, the calculated indirect band gap of the bulk sample (**Fig. 3**b) is 2.54 eV, which is above the values measured in reported literature of 2.12 eV[36] and 2.20 eV[20]. Theory predicts an increase of the band gap by 460 meV from bulk to monolayer (**Fig. 3**b) that agrees with the increased band gap of the exfoliated material compared to the bulk material.[21, 23-24]

The band edge alignment with the electrochemical potentials of the water splitting reaction is another significant factor to overall PEC efficiency; the measurements were done by electrochemical Mott–Schottky analysis. As shown in **Fig. 3**c, exfoliated $Pd_3(PS_4)_2$ shows an n-type semiconducting character with a flat band position of -0.83 V (*vs*. SSCE) in 0.5 M $Na_2SO_4$ aqueous solution (pH=7.0) at the frequency range from 100 to 200 Hz, which correspond to the conduction band minimum (CB) of -0.59 eV *vs*. NHE (pH 7.0).[39] From the band gap, we can estimate the valence band maximum at 1.98 eV *vs*. NHE using the Eq. (2):[40]

$$E_v = E_g + E_c \quad (2)$$

where $E_v$, $E_g$ and $E_c$ are the energies of VB, band gap and CB, respectively. The reduction and oxidation potentials of the HER and OER are at -0.41 V and 0.82 V *vs*. NHE at pH=7, respectively. Thus, the band edges of as-exfoliated $Pd_3(PS_4)_2$ span the electrochemical potentials of the water splitting reaction. This is confirmed by theory, as shown in **Fig. 3**d and summarized in **Table 3** (supporting information), which assigns the vacuum-energy corrected valence band maximum of the bulk material to

-0.13 eV relative to the absolute electrode potential of the hydrogen electrode, which matches the measured valence band maximum at -0.18 eV.

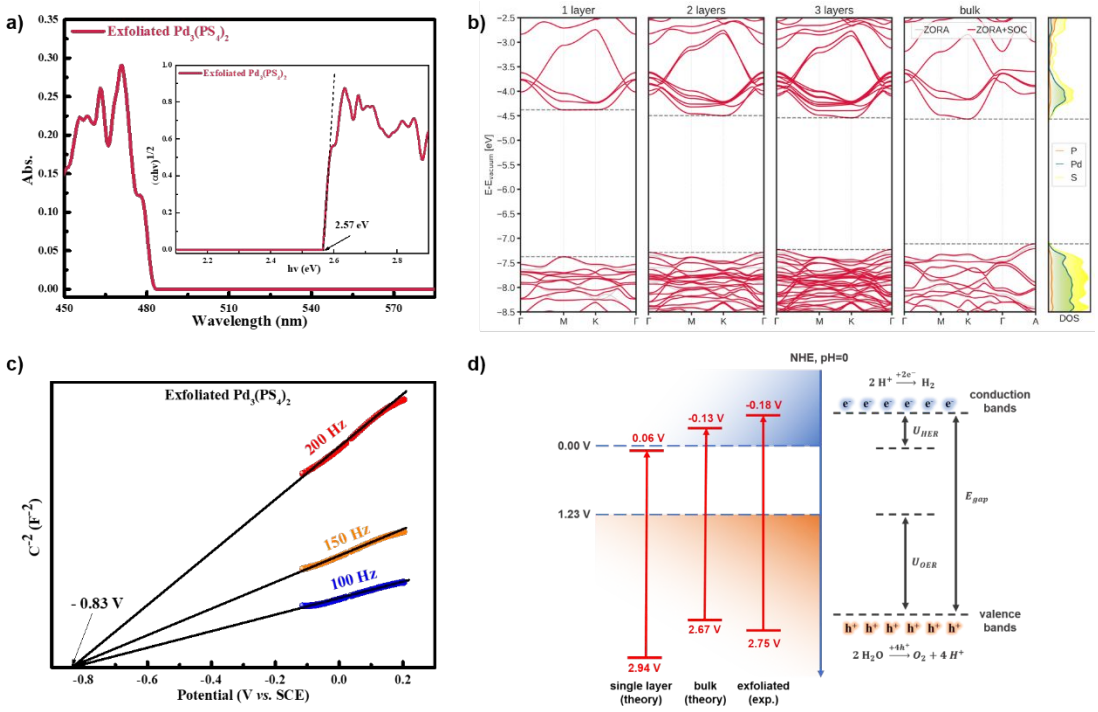


**Figure 3** (a) UV-Vis absorption spectra and (b) vacuum-corrected band structures for different layer numbers of $Pd_3(PS_4)_2$ at the HSE06 level of theory including SOC. (c) Mott-Schottky plots of exfoliated $Pd_3(PS_4)_2$ under frequencies of 100 to 200 Hz at 0.5 M $Na_2SO_4$ (pH 7.0) aqueous solution. (d) schematic diagram of PEC water splitting of exfoliated $Pd_3(PS_4)_2$ photoelectrode based on Mott-Schottky and band edge. Note that the valence band energies are given with positive signs, such that the band gap is $E_g = E_v + E_c$.

As the interfacial electron transfer efficiency is essential for the PEC water splitting process, the electrochemical impedance spectra (EIS) are compared for the bulk and exfoliated $Pd_3(PS_4)_2$ at different pH values. Compared to bulk samples, the smaller arc radius in the Nyquist plots (**Fig. 4**a-c) of exfoliated $Pd_3(PS_4)_2$ nanosheets under irradiation means lower electron transfer resistance, revealing a faster electron transfer process under each pH condition of 0.5 M $H_2SO_4$, 1 M PBS (pH 7.0) and 1 M KOH. Additionally, the arc radius is smallest under acidic conditions for each measured

sample, indicating fast electron transfer, while the larger arc radius occurring in neutral conditions indicates slower electron transfer. The transient photocurrent responses of materials were recorded through multiple on/off light (420 nm violet light) irradiation cycles under different pH conditions at constant potentials of both -0.4 V (vs. RHE) (for HER) and +2 V (vs. RHE) (for OER). As shown in **Fig. 4**d-e, the photocurrent density of $Pd_3(PS_4)_2$ nanosheets electrodes are higher than bulk $Pd_3(PS_4)_2$ electrodes in our experimental conditions. As the photocurrent response within electrodes is bound to the separation efficiency of photogenerated electron-hole pairs,[41] the higher photocurrent suggests low electron-hole pair recombination and a higher electron transfer efficiency for exfoliated $Pd_3(PS_4)_2$ nanosheets. Notably, the detected photocurrent density under neutral conditions is lower than under alkaline and acidic conditions for the measurements of both -0.4 V (vs. RHE) and +2 V (vs. RHE), and the photocurrent density is higher in an acidic environment compared to an alkaline environment in the -0.4 V (*vs*. RHE) measurement. We could conclude from the characterizations of EIS and transient photocurrent responses that exfoliated $Pd_3(PS_4)_2$ nanosheets show a faster electron transfer process and higher photogenerated electron transfer efficiency than its bulk counterpart, and the most efficient reaction environment for PEC water splitting might be under acidic conditions.

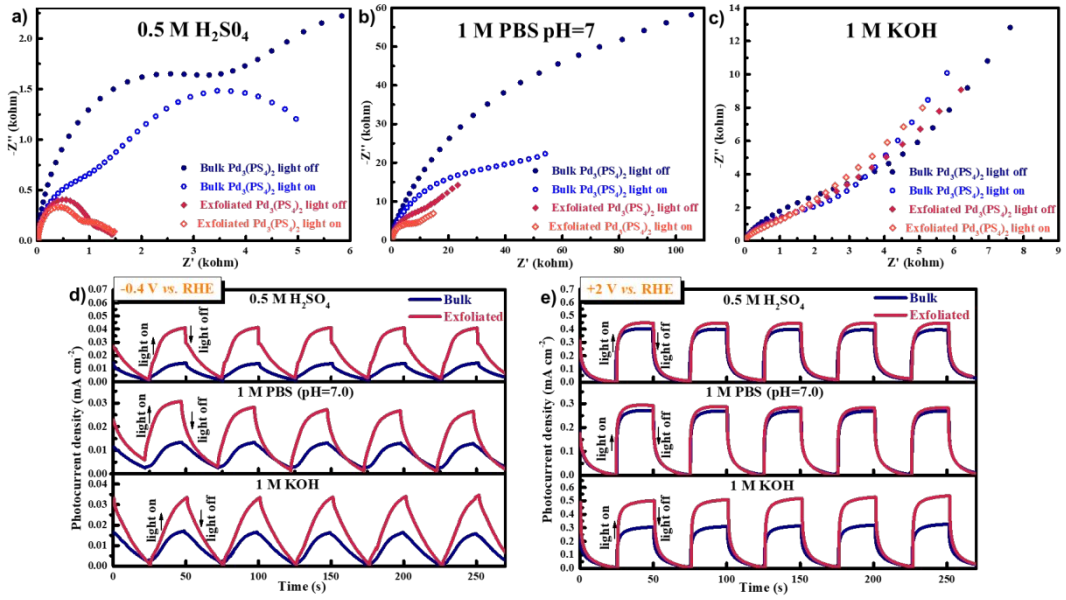


**Figure 4** Electrochemical impedance Nyquist plots of bulk and exfoliated $Pd_3(PS_4)_2$ under 420 nm irradiation at different pH values of (a) 0.5 M $H_2SO_4$, (b) 1 M phosphate buffer solution (pH=7.0) and (c) 1M KOH aqueous solution; (d) and (e) transient photocurrent responses of materials under different pH range at -0.4 V and +2 V (*vs*. RHE ), respectively. The collected photocurrent density is multiplied by -1 for the measurements at -0.4 V (*vs*. RHE).

We further performed OER and HER measurements of both bulk and exfoliated $Pd_3(PS_4)_2$ at acidic, neutral and alkaline pH. As shown in **Fig. 5**a-d, the exfoliated $Pd_3(PS_4)_2$ nanosheets exhibit better electrocatalytic performance than their bulk counterparts. **Fig. 5**a shows that the irradiated $Pd_3(PS_4)_2$ nanosheets demonstrate excellent HER activity with an overpotential of 412 mV at 10 mA $cm^{-2}$ in 0.5 M $H_2SO_4$. In contrast, its OER activity is weakly expressed due to the slight decrease of the overpotential barrier from 955 to 914 mV. In **Fig. 5**b, the HER and OER with $Pd_3(PS_4)_2$ nanosheets under irradiation show overpotentials of 890 mV and 1029 mV in 1 M PBS (pH 7.0), respectively. In an alkaline environment with 1 M KOH, the HER is only weakly catalyzed by both bulk and exfoliated samples (**Fig. 5**c). To compare the PEC activity of $Pd_3(PS_4)_2$ catalysts, we analyzed the overpotential in various pH

environment at a current density of 10 mA $cm^{-2}$ (**Fig. 5**d), where the PEC activity of commercial Pt/C under ambient conditions was used as reference (corresponding LSV curves shown in Fig. S6a). Both OER and HER activity of exfoliated $Pd_3(PS_4)_2$ nanosheets are superior to their bulk counterparts. Under irradiation at 420 nm, the HER overpotentials for as-prepared $Pd_3(PS_4)_2$ nanosheets are 0.41 V (pH 0), 0.89 V (pH 7.0) and 0.66 V (pH=14), respectively, which can nearly compete with the commercial Pt/C electrode with HER overpotentials of 0.38 mV, 0.87 mV and 0.64 mV.

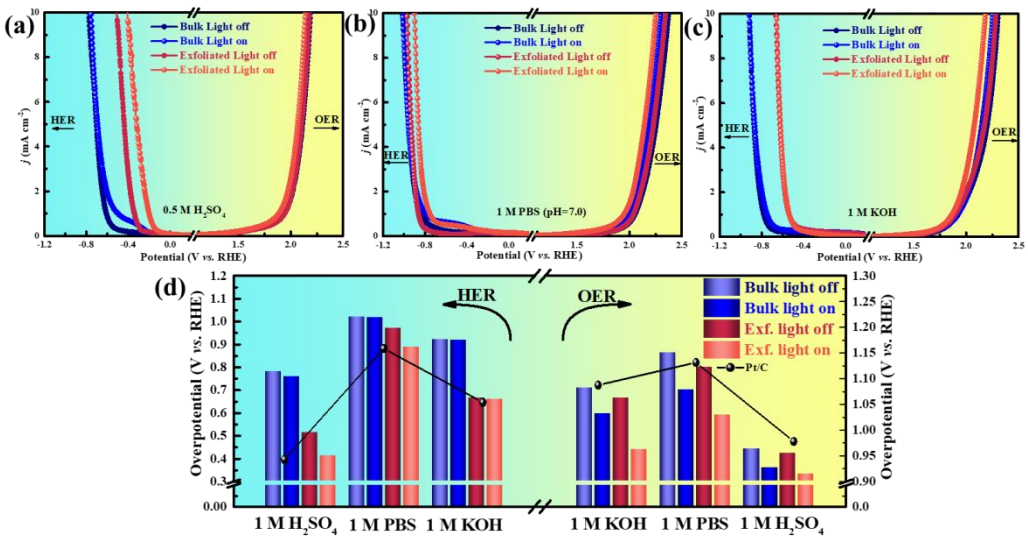


**Figure 5** The PEC water splitting studies of bulk and exfoliated $Pd_3(PS_4)_2$: polarization curves of bulk and exfoliated samples for HER and OER at (a) 0.5 M $H_2SO_4$, (b) 1 M phosphate buffer solution (pH 7.0) and (c) 1M KOH aqueous solution, respectively. (d) Comparison of the overpotential of PEC water splitting at 10 mA $cm^{-2}$. The collected current density (*j*) is multiplied by -1 for HER.

## Conclusion

In summary, a novel two-dimensional semiconductor material $Pd_3(PS_4)_2$ was successfully exfoliated by lithium intercalation and ultrasonication from its bulk counterpart. The band gap of the as-exfoliated material was estimated at 2.57 eV; this indicates the ability of the material to absorb in the visible light and further use it in

photoelectrocatalysis. The as-exfoliated $Pd_3(PS_4)_2$ nanosheets demonstrate their dual photoelectrocatalytic activity as electrodes for HER and OER. The photo-induced water splitting of the $Pd_3(PS_4)_2$ nanosheets works best in an acidic environment. This new exfoliated 2D $Pd_3(PS_4)_2$ might enrich the database of materials applied in the field of photoelectrocatalysis.

**Reference**

(1) Faraji, M.; Yousefi, M.; Yousefzadeh, S.; Zirak, M.; Naseri, N.; Jeon, T. H.; Choi, W.; Moshfegh, A. Z. Two-dimensional materials in semiconductor photoelectrocatalytic systems for water splitting. *Energy & Environmental Science* **2019,** *12* (1), 59-95.

(2) Guo, Z.; Zhou, J.; Zhu, L.; Sun, Z. MXene: a promising photocatalyst for water splitting. *Journal of Materials Chemistry A* **2016,** *4* (29), 11446-11452.

(3) Rahman, M. Z.; Kwong, C. W.; Davey, K.; Qiao, S. Z. 2D phosphorene as a water splitting photocatalyst: fundamentals to applications. *Energy & Environmental Science* **2016,** *9* (3), 709-728.

(4) Zhang, J.; Wang, T.; Pohl, D.; Rellinghaus, B.; Dong, R.; Liu, S.; Zhuang, X.; Feng, X. Interface engineering of $MoS_2/Ni_3S_2$ heterostructures for highly enhanced electrochemical overall-water-splitting activity. *Angewandte Chemie International Edition* **2016,** *55* (23), 6702-6707.

(5) Ida, S.; Ishihara, T. Recent Progress in Two-Dimensional Oxide Photocatalysts for Water Splitting. *The Journal of Physical Chemistry Letters* **2014,** *5* (15), 2533-2542, DOI: 10.1021/jz5010957.

(6) Wang, H.; Zhang, X.; Xie, Y. Recent progress in ultrathin two-dimensional semiconductors for photocatalysis. *Materials Science and Engineering: R: Reports* **2018,** *130*, 1-39.

(7) Ni, M.; Leung, M. K. H.; Leung, D. Y. C.; Sumathy, K. A review and recent developments in photocatalytic water-splitting using $TiO_2$ for hydrogen production. *Renewable and Sustainable Energy Reviews* **2007,** *11* (3), 401-425.

(8) She, X.; Wu, J.; Xu, H.; Zhong, J.; Wang, Y.; Song, Y.; Nie, K.; Liu, Y.; Yang, Y.; Rodrigues, M. T. F. High Efficiency Photocatalytic Water Splitting Using 2D α - $Fe_2O_3$/g-$C_3N_4$ Z-Scheme Catalysts. *Advanced Energy Materials* **2017,** *7* (17), 1700025.

(9) Liu, Q.; Lu, H.; Shi, Z.; Wu, F.; Guo, J.; Deng, K.; Li, L. 2D ZnIn2S4 nanosheet/1D TiO2 nanorod heterostructure arrays for improved photoelectrochemical water splitting. *ACS applied materials & interfaces* **2014,** *6* (19), 17200-17207.

(10) Li, Y.; Li, Y.-L.; Sa, B.; Ahuja, R. Review of two-dimensional materials for photocatalytic water splitting from a theoretical perspective. *Catalysis Science & Technology* **2017,** *7* (3), 545-559.

(11) Yin, Z.; Chen, B.; Bosman, M.; Cao, X.; Chen, J.; Zheng, B.; Zhang, H. Au

nanoparticle‐modified $MoS_2$ nanosheet‐based photoelectrochemical cells for water splitting. *Small* **2014,** *10* (17), 3537-3543.
(12) Xie, G.; Zhang, K.; Guo, B.; Liu, Q.; Fang, L.; Gong, J. R. Graphene‐based materials for hydrogen generation from light‐driven water splitting. *Advanced materials* **2013,** *25* (28), 3820-3839.
(13) Yang, Y.; Fei, H.; Ruan, G.; Li, Y.; Tour, J. M. Vertically aligned $WS_2$ nanosheets for water splitting. *Advanced Functional Materials* **2015,** *25* (39), 6199-6204.
(14) Jia, Y.; Zhang, L.; Gao, G.; Chen, H.; Wang, B.; Zhou, J.; Soo, M. T.; Hong, M.; Yan, X.; Qian, G. A heterostructure coupling of exfoliated Ni-Fe hydroxide nanosheet and defective graphene as a bifunctional electrocatalyst for overall water splitting. *Advanced Materials* **2017,** *29* (17), 1700017.
(15) Qiao, M.; Liu, J.; Wang, Y.; Li, Y.; Chen, Z. $PdSeO_3$ monolayer: promising inorganic 2D photocatalyst for direct overall water splitting without using sacrificial reagents and cocatalysts. *Journal of the American Chemical Society* **2018,** *140* (38), 12256-12262.
(16) Liu, G.; Li, Z.; Hasan, T.; Chen, X.; Zheng, W.; Feng, W.; Jia, D.; Zhou, Y.; Hu, P. Vertically aligned two-dimensional $SnS_2$ nanosheets with a strong photon capturing capability for efficient photoelectrochemical water splitting. *Journal of Materials Chemistry A* **2017,** *5* (5), 1989-1995.
(17) Yu, L.; Zhou, H.; Sun, J.; Qin, F.; Yu, F.; Bao, J.; Yu, Y.; Chen, S.; Ren, Z. Cu nanowires shelled with NiFe layered double hydroxide nanosheets as bifunctional electrocatalysts for overall water splitting. *Energy & Environmental Science* **2017,** *10* (8), 1820-1827.
(18) Liu, H.; Xu, B.; Liu, J. M.; Yin, J.; Miao, F.; Duan, C.-G.; Wan, X. G. Highly efficient and ultrastable visible-light photocatalytic water splitting over $ReS_2$. *Physical Chemistry Chemical Physics* **2016,** *18* (21), 14222-14227.
(19) Peng, R.; Ma, Y.; Huang, B.; Dai, Y. Two-dimensional Janus PtSSe for photocatalytic water splitting under the visible or infrared light. *Journal of materials chemistry A* **2019,** *7* (2), 603-610.
(20) Bither, T. A.; Donohue, P. C.; Young, H. S. Palladium and platinum phosphochalcogenides—synthesis and properties. *Journal of Solid State Chemistry* **1971,** *3* (2), 300-307.
(21) Jing, Y.; Heine, T. Two-dimensional $Pd_3P_2S_8$ semiconductors as photocatalysts for the solar-driven oxygen evolution reaction: a theoretical investigation. *Journal of Materials Chemistry A* **2018,** *6* (46), 23495-23501.
(22) Zhang, X.; Luo, Z.; Yu, P.; Cai, Y.; Du, Y.; Wu, D.; Gao, S.; Tan, C.; Li, Z.; Ren, M. Lithiation-induced amorphization of $Pd_3P_2S_8$ for highly efficient hydrogen evolution. *Nature Catalysis* **2018,** *1* (6), 460-468.
(23) Tang, C.; Zhang, C.; Matta, S. K.; Jiao, Y.; Ostrikov, K.; Liao, T.; Kou, L.; Du, A. Predicting new two-dimensional Pd3 (PS4) 2 as an efficient photocatalyst for water splitting. *The Journal of Physical Chemistry C* **2018,** *122* (38), 21927-21932.
(24) Shan, Y.; Li, T.; Liu, L. Electronic structure and optical characteristic for $Pd_3P_2S_8$ layers. *Solid State Communications* **2020,** *306*, 113786.
(25) Ghorai, A.; Midya, A.; Maiti, R.; Ray, S. K. Exfoliation of $WS_2$ in the

semiconducting phase using a group of lithium halides: a new method of Li intercalation. *Dalton Transactions* **2016,** *45* (38), 14979-14987.
(26) Larson, A. C.; Von Dreele, R. B. General structure analysis system, report LAUR 86-748. *Los Alamos National Laboratory, NM* **1994,** *16*.
(27) Rietveld, H. M. The Rietveld Method? A Historical Perspective. *Australian Journal of Physics* **1988,** *41* (2), 113-116.
(28) Blum, V.; Gehrke, R.; Hanke, F.; Havu, P.; Havu, V.; Ren, X.; Reuter, K.; Scheffler, M. Ab initio molecular simulations with numeric atom-centered orbitals. *Computer Physics Communications* **2009,** *180* (11), 2175-2196.
(29) Perdew, J. P.; Burke, K.; Ernzerhof, M. D. of Physics and NOL 70118 J. Quantum theory group Tulane University. *Phys. Rev. Lett* **1996,** *77*, 3865-3868.
(30) Tkatchenko, A.; Ambrosetti, A.; DiStasio Jr, R. A. Interatomic methods for the dispersion energy derived from the adiabatic connection fluctuation-dissipation theorem. *The Journal of chemical physics* **2013,** *138* (7), 074106.
(31) Heyd, G. E. Scuseria, and M. Ernzerhof. *J. Chem. Phys* **2003,** *118* (18), 8207.
(32) Maschio, L.; Kirtman, B.; Rérat, M.; Orlando, R.; Dovesi, R. Ab initio analytical Raman intensities for periodic systems through a coupled perturbed Hartree-Fock/Kohn-Sham method in an atomic orbital basis. I. Theory. *The Journal of chemical physics* **2013,** *139* (16), 164101.
(33) Dovesi, R.; Erba, A.; Orlando, R.; Zicovich-Wilson, C. M.; Civalleri, B.; Maschio, L.; Rérat, M.; Casassa, S.; Baima, J.; Salustro, S. Wiley Interdiscip. *Rev.: Comput. Mol. Sci* **2018,** *8*, e1360.
(34) Kim, C.; Nguyen, T. P.; Le, Q. V.; Jeon, J. M.; Jang, H. W.; Kim, S. Y. Performances of liquid‐exfoliated transition metal dichalcogenides as hole injection layers in organic light‐emitting diodes. *Advanced Functional Materials* **2015,** *25* (28), 4512-4519.
(35) Huang, P.; Wang, Z.; Liu, Y.; Zhang, K.; Yuan, L.; Zhou, Y.; Song, B.; Li, Y. Water-soluble 2D transition metal dichalcogenides as the hole-transport layer for highly efficient and stable p-i-n perovskite solar cells. *ACS applied materials & interfaces* **2017,** *9* (30), 25323-25331.
(36) Calareso, C.; Grasso, V.; Silipigni, L. Vibrational and low-energy optical spectra of the square-planar $Pd_3$ $(PS_4)_2$ thiophosphate. *Physical Review B* **1999,** *60* (4), 2333.
(37) Grasso, V.; Silipigni, L. X-ray photoemission spectra and x-ray excited Auger spectrum investigation of the electronic structure of $Pd_3(PS_4)_2$. *Journal of Vacuum Science & Technology A: Vacuum, Surfaces, and Films* **2003,** *21* (4), 860-865.
(38) Latiff, N. M.; Mayorga-Martinez, C. C.; Khezri, B.; Szokolova, K.; Sofer, Z.; Fisher, A. C.; Pumera, M. Cytotoxicity of layered metal phosphorus chalcogenides (MPXY) nanoflakes; $FePS_3$, $CoPS_3$, $NiPS_3$. *FlatChem* **2018,** *12*, 1-9.
(39) Li, X.; Yu, J.; Low, J.; Fang, Y.; Xiao, J.; Chen, X. Engineering heterogeneous semiconductors for solar water splitting. *Journal of Materials Chemistry A* **2015,** *3* (6), 2485-2534.
(40) Morrison, S. R. Electrochemistry at semiconductor and oxidized metal electrodes. **1980**.
(41) Wu, D.; Ye, L.; Yip, H. Y.; Wong, P. K. Organic-free synthesis of {001} facet

dominated BiOBr nanosheets for selective photoreduction of $CO_2$ to CO. *Catalysis Science & Technology* **2017,** *7* (1), 265-271.